

## EVOLUTION OF TEMPERATURE DURING SHAPED METAL DEPOSITION: FINITE ELEMENT PREDICTIONS VS. OBSERVATIONS

Víctor D. Fachinotti<sup>a</sup>, Alberto Cardona<sup>a</sup>, Alejandro Cosimo<sup>a</sup>,  
Bernd Baufeld<sup>b</sup> and Omer Van der Biest<sup>b</sup>

<sup>a</sup>*Centro Internacional de Métodos Computacionales en Ingeniería (CIMEC), Instituto de Desarrollo Tecnológico para la Industria Química (INTEC), Universidad Nacional del Litoral (UNL)/ Consejo Nacional de Investigaciones Científicas y Técnicas (CONICET), Predio CCT-CONICET Santa Fe, Ruta 168, Paraje El Pozo, 3000 Santa Fe, Argentina, vfachino@intec.unl.edu.ar, acardona@intec.unl.edu.ar, alecosimo@gmail.com, <http://www.cimec.org.ar>*

<sup>b</sup>*Department of Metallurgy and Materials Engineering (MTM), Katholieke Universiteit Leuven (KUL), Kasteelpark Arenberg 44, 3001 Leuven, Belgium, Bernd.Baufeld@mtm.kuleuven.be, Omer.VanderBiest@mtm.kuleuven.be, <http://www.mtm.kuleuven.be>*

**Keywords:** Shaped metal deposition, finite element, temperature evolution.

**Abstract.** Shaped Metal Deposition (SMD) is a novel technology to build near-net shaped parts by successive weld deposition. The SMD rig consists of a robot with a Tungsten Inert Gas (TIG) welding torch and a manipulator, which are housed inside a sealed chamber. The heat transfer problem is modeled in a series of walls made by SMD of Ti-6Al-4V alloy. The studied specimens have different dimensions and were obtained using a wide range of process parameters (number of layers, layer height, wire feed rate, travel speed, heat input, etc.). The aim is to correlate the temperature field predicted using the finite element model developed by Centro Internacional de Métodos Computacionales en Ingeniería (Santa Fe, Argentina) to macro-, meso- and micrographical observations done at the Department of Metallurgy and Materials Engineering (Katholieke Universiteit Leuven, Belgium), as a way of validating the model of such a complex process.

SMD subjects the build part repeatedly to a specific temperature field which results in a unique morphology and in microstructures usually not achievable by conventional fabrication techniques. The appearance of distinct microstructures in the top of the walls, in the substrate and in the intermediate region is explained on the basis of temperature and temperature rate results.

Modelling of microstructure evolution in terms of phase kinetics based on phase transformation diagrams is dealt with in a companion paper.

## 1 INTRODUCTION

Shaped Metal Deposition (SMD) is a novel rapid prototyping technique to build near-net shape metal pieces, which allows avoiding time and material intensive machining. The SMD rig consists of a welding robot with a TIG torch housed in an argon filled chamber and the material is supplied by wire which is fed into the chamber through an annular feed pipe. The robot follows a computer aided design (CAD) code in order to make the desired piece by the deposition of successive weld layers.

SMD usually takes tens of minutes to several hours to build a typical piece depositing tens to hundreds of layers. SMD involves a moving and localized heat source and subjects the build part to a specific temperature field. Specifically, each location experiences repeatedly heating and cooling with high rates up to maximum temperatures, which may depend on the time and location. For example, during the deposition of a new layer, two or three of the previous layers are re-melted. Hence, SMD results in a unique morphology and in microstructures, usually not achievable by conventional fabrication techniques (Baufeld et al., 2009a). The mechanical properties, depending on the microstructure, may vary therefore for different locations (Baufeld et al., 2009b). Furthermore, the applied SMD parameters also influence the properties of the parts (Baufeld et al., 2010a and 2010b). It is therefore of utterly importance for application to predict the variation of the microstructure with location and SMD parameters requiring the modeling of the complex temperature field during the SMD process.

## 2 THE HEAT TRANSFER PROBLEM IN SMD

Figure 1 shows exemplarily a piece made by SMD of Ti-6Al-4V alloy, with the typical shape addressed in this work: square tubes with different dimensions, built by varying the main process parameters (arc current and voltage, welding speed, wire feed rate, number of layers) within a wide range, as seen in Table 1.

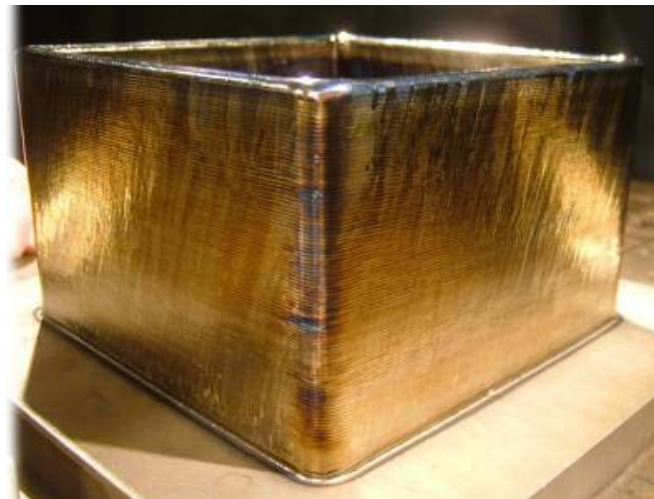


Figure 1: Square cylinder produced by SMD.

ID #	Thickness $w$ [mm]	Side length [mm]	Total height $h$ [mm]	Number of layers $N$	Current [A]	Voltage [V]	Wire feed rate $V_f$ [mm/min]	Welding velocity $V_w$ [mm/min]
21	9.45	140	70	70	182.5	12.8	2200	250
22	9.49	140	70	87	164.7	11.2	1400	250
23	8.75	140	70	87	163.4	11.6	1800	300
24	9.87	140	70	70	183.2	12.4	2400	300
35	9.67	140	70	70	182.5	12.8	2200	300
50	19.80	100	25	50	221.4	11.5	770	100

Table 1: Geometrical data and process parameters used to build the selected samples.

Figure 2 depicts etched cross-sections of optical macrographs taken from the walls of the parts selected for this study. In all of them, we can distinguish a top region with fine  $\alpha$  lamellae within a  $\beta$  matrix, and a bottom region characterised by the presence of bands parallel to the base, where the  $\alpha$  phase lamellae are coarser. According to Baufeld et al. (2009a), the top region represents the area where the peak temperature has exceeded the  $\beta$ -transus temperature  $T_\beta$  during the last pass. In other words, this top region embodies the fusion zone (FZ) consisting of the material whose peak temperature has exceeded the solidus temperature  $T_{sol}$ , plus the heat affected zone (HAZ) where the maximal temperature ranges between  $T_\beta$  and  $T_{sol}$ .



Figure 2: Optical macrographs of cross sections of selected walls made by SMD (the scale varies).

Hence, in order to determine the extension of this top region, the evolution of temperatures in a domain consisting of the base plate (also Ti-6Al-4V in this case) and the wall, which grows

gradually, layer by layer, all along the deposition process, must be computed. To do this, ideally a fully three-dimensional heat transfer problem should be solved. However, the cost of such analysis is usually unaffordable for complex processes such like in welding and especially here: time steps of  $O(0.1 \text{ sec})$  are required for tracking the highly concentrated welding heat source with enough accuracy (Zhang et al., 2003), while the fabrication of the considered pieces takes about 2.5 to 4 hours.

Computational time is significantly reduced by assuming heat flow restricted to the cross section, such that a two-dimensional model can be used. In this case, a typical cross section far enough from the edges of the cylinder is considered. Please note that macrographs in Figure 2 were taken from such cross sections.

The accuracy of this model increases with the Peclet number (Mendez, 1995; Goldak and Akhlagh, 2005), defined as

$$Pe = \frac{V_w l}{\alpha} \quad (1)$$

where  $V_w$  is the welding velocity (see Table 1),  $l$  is the characteristic dimension in the welding direction, and  $\alpha$  is the thermal diffusivity. Considering that Ti-6Al-4V has an average diffusivity of  $4 \times 10^6 \text{ m}^2/\text{s}$  in the high temperature range concerned by welding and taking as characteristic dimension the side length (given in Table 1), the Peclet number ranges from 41.7 for sample 50 to 187.5 for samples 21, 22 and 23. Since  $Pe \gg 1$ , the cross-sectional model is expected to be accurate enough for the purposes of this work.

Not only the dimension of the problem is considerably reduced by using this cross-sectional model, also the number of time steps is: now, time steps of  $O(0.1 \text{ sec})$  are only required during the few seconds when the welding heat source is crossing the considered section.

Furthermore, it is assumed that the temperature distribution is symmetric with respect to the mid-plane of the wall, which is supported by observing the macrographs in Figure 2, where thermal-driven bands exhibit such symmetry. The geometrical model for the analysis of this type of pieces is illustrated in Figure 3. There,  $\Omega_0$  denotes the base plate subdomain, and  $\Omega_I^{lay}$  ( $I = 1, 2, \dots, N$ ) is the subdomain corresponding to the  $I$ -th layer, which is added to the existing domain  $\Omega_{I-1}$  at a given time instant  $t_I > 0$ . Therefore, at a given time  $t$  in the time interval  $[t_I, t_{I+1})$ , the domain of analysis is  $\Omega_I = \Omega_0 \cup \Omega_1^{lay} \cup \dots \cup \Omega_I^{lay}$ . Let  $\Gamma_I$  be the boundary of  $\Omega_I$ , consisting of a portion  $\Gamma_I^{sym}$  laying on the symmetry axis, and hence adiabatic, and a portion  $\Gamma_I^{cr}$  through which the piece exchanges heat with the environment (the sealed Argon-filled chamber) by combined convection and radiation, such that  $\Gamma_I = \Gamma_I^{sym} \cup \Gamma_I^{cr}$  and  $\Gamma_I^{sym} \cap \Gamma_I^{cr} = \emptyset$ .

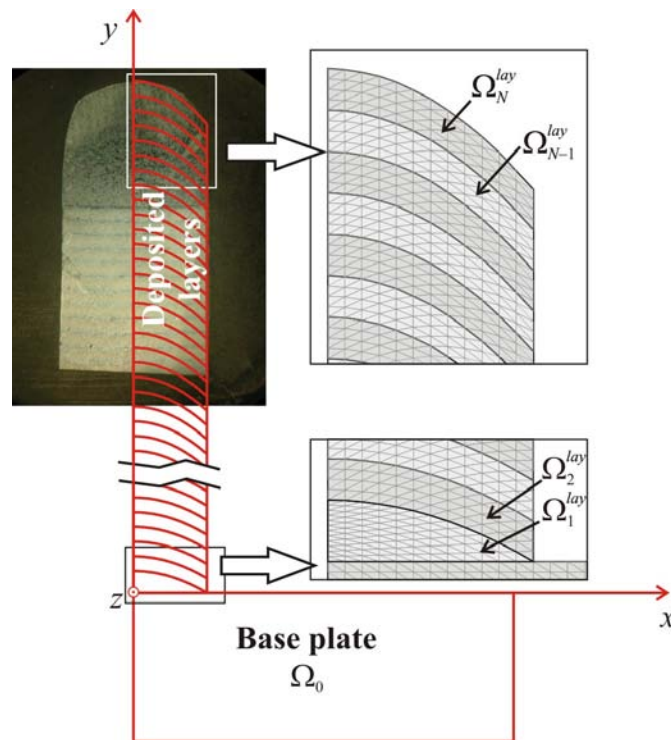


Figure 3: Geometrical model for the analysis of sample 24.

The problem to solve can be then written as: find the temperature  $T = T(x, y, t)$  at any point  $(x, y) \in \Omega_I$  at the instant  $t \in (t_l, t_{l+1}), t > 0$ , satisfying the transient heat conduction equation

$$\frac{\partial H}{\partial t} - \text{div}(\boldsymbol{\kappa} \text{grad } T) = q \quad (2)$$

where  $H = H(T)$  is the enthalpy,  $\boldsymbol{\kappa} = \boldsymbol{\kappa}(T)$  is the thermal conductivity and  $q = q(x, y, t)$  is the heat source representing the welding torch. The heat transfer problem is completed by the initial condition:

$$T(x, y, t_l) = T_l(x, z) \quad \forall (x, y) \in \Omega_I \quad (3)$$

the adiabatic (natural) boundary condition:

$$-\boldsymbol{\kappa} \text{grad } T \cdot \mathbf{n} = 0 \quad \forall (x, y) \in \Gamma_I^{sym} \quad (4)$$

and the convection/radiation (mixed) boundary condition:

$$-\boldsymbol{\kappa} \text{grad } T \cdot \mathbf{n} = h_{cr}(T - T_{cr}) \quad \forall (x, y) \in \Gamma_I^{cr} \quad (5)$$

where  $\mathbf{n}$  is the unit vector pointing outwards and normal to  $\Gamma$ ,  $h_{cr}$  the convection/radiation coefficient (in general, dependent of temperature), and  $T_{cr}$  is either the temperature of the environment or that of the radiant body (assumed to be equal).

A temperature-based formulation is obtained by introducing the enthalpy function defined as follows

$$H(T) = \int_0^T \rho c_p(\tau) d\tau + \rho L f_{liq}(T) \quad (6)$$

where  $\rho c_p$  is the heat capacity,  $L$  the latent heat of solidification and  $f_{liq}$  the volume fraction

of liquid. Following Rai et al. (2007), this fraction is assumed to vary linearly with temperature between the solidus temperature  $T_{sol}$  and the liquidus temperature  $T_{liq}$ , i.e.:

$$f_{liq}(T) = \begin{cases} 0 & \text{if } T \leq T_{sol} \\ \frac{T - T_{sol}}{T_{liq} - T_{sol}} & \text{if } T_{sol} < T < T_{liq} \\ 1 & \text{if } T > T_{liq} \end{cases} \quad (7)$$

Enthalpy should also account for the latent heat involved in solid phase transformations, but this is assumed to be negligible compared to the latent heat of fusion in Ti-6Al-4V (Robert, 2007).

Following Zhuk et al. (2007), the increased heat transfer in the weld pool due to convection effects is modelled here by adopting an artificially increased conductivity for the molten metal.

## 2.1 Arc-welding heat source model

The heat source in welding is often described using the double-ellipsoidal model proposed by Goldak et al. (1984) schematised in Figure 4, where the heat power density is defined as:

$$q_{Goldak}(x', y', z') = \frac{6\sqrt{3}Q}{\pi\sqrt{\pi}ab} \times \begin{cases} \frac{f_f}{c_f} \exp\left(-3\frac{x'^2}{a^2} - 3\frac{y'^2}{b^2} - 3\frac{z'^2}{c_f^2}\right) & \text{for } z' > 0 \\ \frac{f_r}{c_r} \exp\left(-3\frac{x'^2}{a^2} - 3\frac{y'^2}{b^2} - 3\frac{z'^2}{c_r^2}\right) & \text{for } z' < 0 \end{cases} \quad (8)$$

where  $Q$  is the total heat input, and  $O'-x'y'z'$  is a moving orthogonal system of coordinates with origin  $O'$  coinciding with the trace of the torch onto the surface of the weld, the  $z'$ -axis pointing along the welding direction, the  $x'$ -axis lying on the weld surface and the  $y'$ -axis defining the depth;  $a, b, c_f$  (respectively  $c_r$ ) are the semi-axes of the front (respectively rear) semi-ellipsoid,  $f_f$  (respectively  $f_r$ ) is the portion of heat distributed on the front (respectively rear) semi-ellipsoid, with  $f_f + f_r = 2$ . We require the continuity of  $q(x', y', z')$  at  $z' = 0$ , which holds if  $f_f/c_f = f_r/c_r$ , although this was not required by Goldak et al. (1984) in their original work.

Goldak's model was originally developed for welding without filler material, and hence it is appropriate to describe SMD before deposition, i.e., during the so-called TIG-wash stage where several welding passes (typically 3 to 6) are made in order to preheat the substrate.

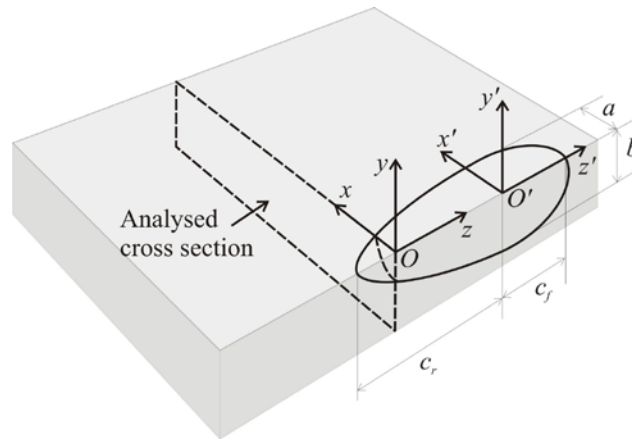


Figure 4: Double-ellipsoidal heat source (Goldak et al., 1984).

Let  $z = z(t)$  be the position of the welding torch relative to the considered cross section, such that  $z < 0$  (or  $z > 0$ ) before (or after) the pass of the torch through this section,  $x \equiv x'$  and  $y \equiv y'$ , as shown on Figure 4. Note that  $z = -z'$  for all the points in the cross section. The heat power density at each point  $(x, y) \in \Omega \equiv \Omega_0$  (i.e., within the substrate) at the instant  $t < t_1$  is

$$q_0(x, y, t) = \frac{6\sqrt{3}Q}{\pi\sqrt{\pi}ab} \times \begin{cases} \frac{f_f}{c_f} \exp\left(-3\frac{x^2}{a^2} - 3\frac{y^2}{b^2} - 3\frac{z(t)^2}{c_f^2}\right) & \text{for } z(t) < 0 \\ \frac{f_r}{c_r} \exp\left(-3\frac{x^2}{a^2} - 3\frac{y^2}{b^2} - 3\frac{z(t)^2}{c_r^2}\right) & \text{for } z(t) > 0 \end{cases} \quad (9)$$

Then, the total heat power distributed on the considered cross section when the torch is located at  $z = z(t)$  is

$$\int_0^\infty \int_{-\infty}^\infty q_0(x, y, t) dx dy = \frac{\sqrt{3}Q}{\sqrt{\pi}} \times \begin{cases} \frac{f_f}{c_f} \exp\left(-3\frac{z(t)^2}{c_f^2}\right) & \text{for } z(t) < 0 \\ \frac{f_r}{c_r} \exp\left(-3\frac{z(t)^2}{c_r^2}\right) & \text{for } z(t) > 0 \end{cases} \quad (10)$$

This equation is also valid during the deposition stage ( $t \geq t_1$ ). However, it is not longer easy to choose a function to describe its distribution across the section since the surface of the weld does not longer coincide with the plane  $y' = 0$ . Furthermore, the double-ellipsoidal geometry adopted by Goldak's model is supposed to reproduce the shape of the weld pool, which is not the case for multilayered walls (e.g., sample 22 in Figure 5).

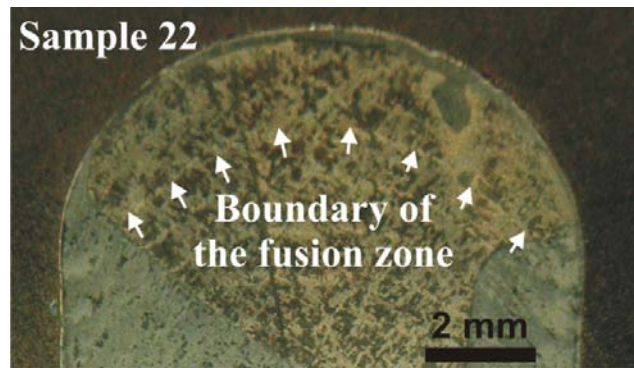


Figure 5: Location of the boundary of the fusion zone in sample 22.

Until a deeper study of the weld pool including fluid flow be undertaken (up to now, these studies are restricted to welding without deposition, see for instance Rai et al., 2007), for the sake of simplicity it has to be assumed that the heat power is uniformly distributed throughout the last added material only. Then, at each point  $(x, y) \in \Omega_I^{lay}$  at time  $t \in [t_I, t_{I+1})$ , the heat power density is defined as

$$q_I(t) = \frac{\sqrt{3}Q}{\sqrt{\pi}\Omega_I^{lay}} \times \begin{cases} \frac{f_f}{c_f} \exp\left(-3\frac{z(t)^2}{c_f^2}\right) & \text{for } z(t) < 0 \\ \frac{f_r}{c_r} \exp\left(-3\frac{z(t)^2}{c_r^2}\right) & \text{for } z(t) > 0 \end{cases} \quad (11)$$

## 2.2 Finite element modeling

The finite element model for the solution of the heat conduction equation with phase change has been introduced elsewhere (Fachinotti et al., 1999). A brief description is included here for the sake of completeness. The weak form of the heat conduction equation (Eq. (2)), subject to the boundary conditions (Eqs. (4) and (5)), and supplemented by the constitutive law for the enthalpy (Eq. (6)) can be written as follows: find  $T \in \mathcal{V}$  such that

$$\begin{aligned} \int_{\Omega_I} \rho c_p \frac{\partial T}{\partial t} w \, dV + \int_{\Omega_I} \kappa \text{grad } T \cdot \text{grad } w \, dV \\ + \int_{\Gamma^{cr}} h_{cr}(T - T_{cr})w \, dV + \frac{\partial}{\partial t} \int_{\Omega_I} \rho L f_{liq} w \, dV = \int_{\Omega_I} q w \, dV \end{aligned} \quad (12)$$

for all admissible weighting function  $w$ .

Let us assume  $\Omega_I$  divided into  $n^e$  linear triangular finite elements, yielding a mesh of  $n^n$  nodes. The typical finite element approximation for the solution can be written as:

$$T(x, y, t) \approx \sum_{j=1}^{n^n} N_j(x, y) T_j(t) \quad (13)$$

where  $T_j(t)$  is the temperature at node  $(x_j, y_j)$  and  $N_j(x, y)$  the shape function associated to this node such that  $N_j(x_i, y_i) = \delta_{ij}$ ,  $i, j = 1, 2, \dots, n^n$ .

The standard (Galerkin) finite element formulation assumes further that the weighting functions coincide with the shape functions, yielding

$$\begin{aligned}
 & \underbrace{\left( \int_{\Omega_I} \rho c_p N_i N_j w \, dV \right)}_{C_{ij}} \frac{\partial T_j}{\partial t} + \underbrace{\left( \int_{\Omega_I} \kappa \text{grad } N_i \cdot \text{grad } N_j \, dV \right)}_{K_{ij}} T_j \\
 & \quad + \frac{\partial}{\partial t} \underbrace{\left( \int_{\Omega_I} \rho L f_{liq} N_i \, dV \right)}_{L_i} \\
 & = \underbrace{\int_{\Omega_I} q N_i \, dV}_{F_i^q} - \underbrace{\int_{\Gamma_I^{cr}} h_{cr} N_i (N_j T_j - T_{cr}) \, dV}_{F_i^{cr}}
 \end{aligned} \tag{14}$$

where  $C_{ij}$  is the capacitance (or mass) matrix,  $K_{ij}$  is the conductivity (or stiffness) matrix,  $L_i$  is the latent heat vector,  $F_i^q$  is the welding heat source vector and  $F_i^{cr}$  is the convection-radiation heat flux vector. Capacitance and stiffness matrices as well as the heat flux vector are common of general thermal finite element analysis, and its computation is detailed in many classical books (see for instance, Zienkiewicz and Taylor, 2001). On the contrary, the heat source and the latent heat vector deserve special attention for welding problems.

Before deposition, i.e. when the domain of analysis consists only of the base plate  $\Omega_0$ , heat source is concentrated in a semi-ellipse (the trace of the double-ellipsoidal volume on the cross section). For the accurate apprehension of the steep variation of the heat power density inside this semi-ellipse,  $F_i^{cr}$  is computed over those elements that have at least one node inside the double-ellipsoidal volume using fifth-order Gauss quadrature. During deposition, the heat source is constant over the last added elements and null elsewhere.

Concerning the latent heat vector, the discontinuous integration technique proposed by Fachinotti et al. (1999) is used to compute it on the elements affected by phase change. Let  $\Omega^e$  be a linear triangular finite element affected by phase change, containing a solid subdomain  $\Omega_{sol}^e$ , a mushy subdomain  $\Omega_{mush}^e$  and a liquid subdomain  $\Omega_{liq}^e$ , i.e.,  $\Omega^e = \Omega_{sol}^e \cup \Omega_{mush}^e \cup \Omega_{liq}^e$ . The contribution of such element to the latent heat vector can be computed as

$$\begin{aligned}
 L_i^e &= \int_{\Omega^e} \rho L f_{liq} N_i \, dV \\
 &= \rho L \int_{\Omega_{mush}^e} N_i \frac{N_j T_j - T_{sol}}{T_{liq} - T_{sol}} \, dV + \rho L \int_{\Omega_{liq}^e} N_i \, dV
 \end{aligned} \tag{15}$$

The use of linear triangles allows the analytical computation of this contribution, as described by Fachinotti et al. (1999).

### 2.3 Time integration

The fully implicit, unconditionally stable Euler-backward scheme is used for time integration: once  $T^0 = T(t^0)$  is known,  $T^1 = T(t^1)$  is determined by the following system of algebraic equations:

$$C_{ij}^1 \frac{T_j^1 - T_j^0}{\Delta t} + K_{ij}^1 T_j^1 + \frac{L_i^1 - L_i^0}{\Delta t} = F_i^{q1} + F_i^{cr1} \tag{16}$$

where the super-indices 0 and 1 denote evaluation at time  $t^0$  and  $t^1$ , respectively, and

$\Delta t = t^1 - t^0$  is the time step.

The above equation is highly non-linear mainly due to the latent heat term. For its efficient solution, the exact Newton-Raphson technique is used. The computation of the tangent matrix is detailed in a previous work (Fachinotti et al., 1999).

### 3 RESULTS

The proposed finite element model was applied to the analysis of all the samples shown in Figure 2, which were produced varying the main SMD parameters, as shown in Table 1. We aim to determine the size of the top region, which is defined as the region where the peak temperature exceeded the  $\beta$ -transus  $T_\beta$  during the last welding pass. To this end, the map of the maximal temperature attained during the deposition of the last layer inside the whole domain is determined. The contour curve corresponding to  $T_\beta$  in this map defines the interface between the top and the bottom region. Figure 6 shows the location of this interface for all the studied samples. Numerical results fit qualitatively well what is observed in macrographs. For a quantitative assessment, see Figure 7. This figure indicates that the SMD parameters have a certain and complex influence on the height of the top region, which can be predicted with the help of modelling.

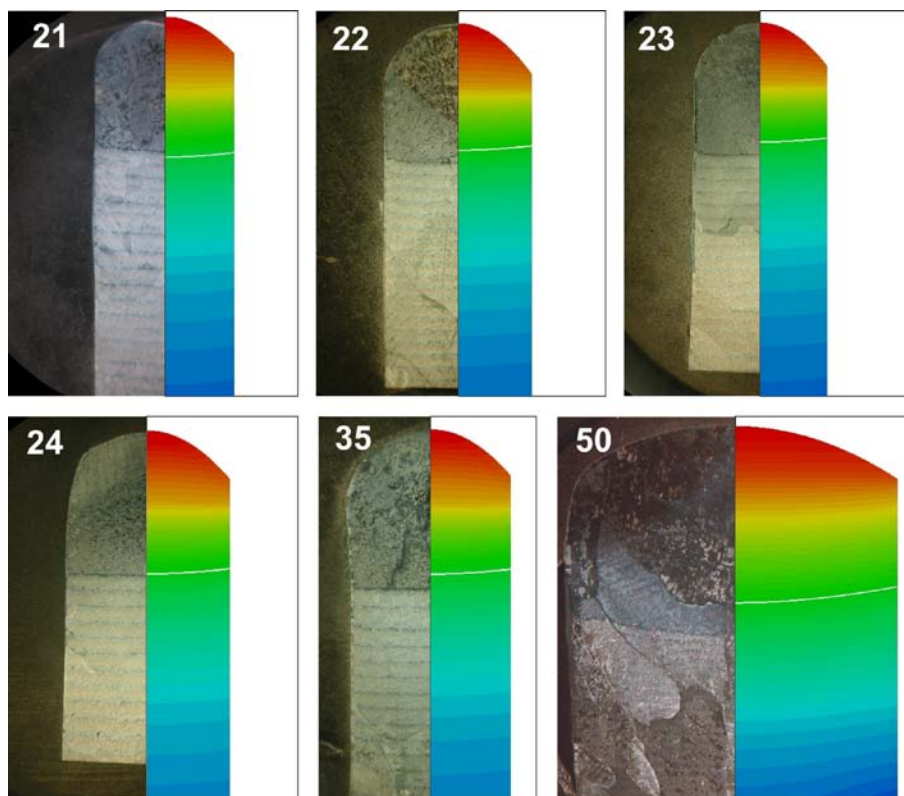


Figure 6: On the right of each sample, maximal temperature attained during the deposition of the last layer, where the contour corresponding to  $\beta$ -transus is highlighted.

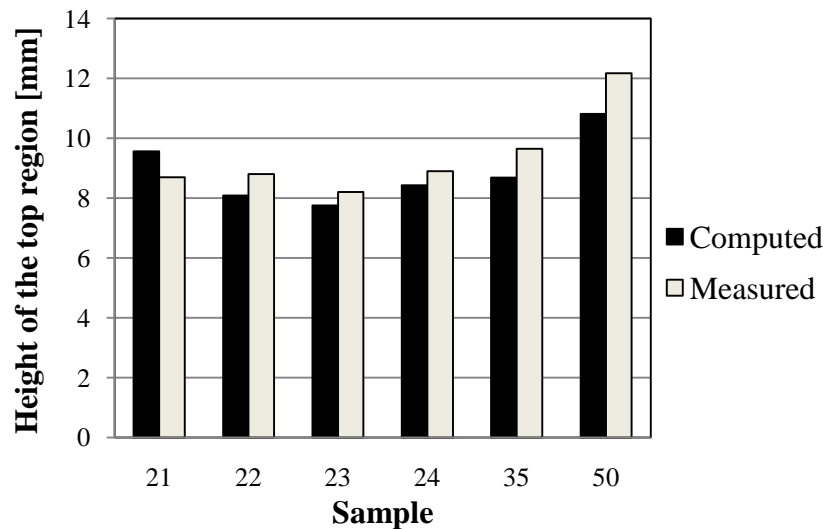


Figure 7: Height of the top region: numerically computed vs. measured from macrographs.

#### 4 CONCLUSIONS

This work gives a first insight of the complex thermal phenomena that take place in the Shaped Metal Deposition (SMD) process, with emphasis on the successful prediction of the extent of the top region.

The numerical simulation of the problem was performed using a 2D cross-section finite element model. The use of a 2D model allows to consider the whole time interval of interest (2-3 hours) using a quite fine time step (0.1 sec) for accuracy reasons.

#### ACKNOWLEDGEMENTS

The support from European Community, contract AST 5-CT 2006-030953, project RAPOLAC (Rapid Production of Large Aerospace Components) of the 6th Framework Programme of the European Commission ([www.RAPOLAC.eu](http://www.RAPOLAC.eu)), CONICET (Consejo Nacional de Investigaciones Científicas y Técnicas, Argentina), and UNL (Universidad Nacional del Litoral, Argentina) is greatly acknowledged.

#### REFERENCES

- Baufeld, B., and Van der Biest O., Mechanical properties of Ti-6Al-4V specimens produced by shaped metal deposition. *Sci. Technol. Adv. Mater.*, doi:10.1088/1468-6996/10/1/015008, 2009a.
- Baufeld, B., Van der Biest, O., and Gault, R., Microstructure of Ti-6Al-4V specimens produced by shaped metal deposition. *International Journal of Materials Research*, 11:1536-1542, 2009b.
- Baufeld, B., Van der Biest, O., Gault, R., and Ridgeway, K., Manufacturing Ti-6Al-4V Components by Shaped Metal Deposition: Microstructure and Mechanical Properties, *TRAM Conference 2009*, Sheffield, UK, IOP Conference Series: Materials Science and Engineering, in press, 2010a.
- Baufeld, B., Brandl, E., and Van der Biest, O., Wire Based Additive Layer Manufacturing: Comparison of Microstructure and Mechanical Properties of Ti-6Al-4V Components fabricated by Laser-beam Deposition and Shaped Metal Deposition, *Journal of Materials Processing Technology*, submitted, 2010b.

- Elmer, J.W., Palmer, T.A., Babu, S.S., Zhang, W., and DebRoy, T., Phase transformation dynamics during welding of Ti-6Al-4V, *J. Appl. Phys.*, 95(12):8327-8339, 2004.
- Fachinotti, V.D., Cardona, A., and Huespe, A.E., A fast convergent and accurate temperature model for phase-change heat conduction. *Int. J. Numer. Methods Engrg.*, 44:1863-1884, 1999.
- Goldak, J. A., and Akhlaghi, M., *Computational Welding Mechanics*. Springer Science+Business Media, Inc., 2005.
- Goldak, J., Chakravarti, A., and Bibby, M., A new finite element model for welding heat sources. *Metallurgical Transactions B*, 15:299-305, 1984.
- Mendez, P.F., Joining metals using semi-solid slurries. Master thesis, Massachusetts Institute of Technology, 1995.
- Rai, R., Elmer, J.W., Palmer, T.A., and DebRoy, T., Heat transfer and fluid flow during keyhole mode laser welding of tantalum, Ti-6Al-4V, 304L stainless steel and vanadium. *J. Phys. D: Appl. Phys.*, 40:5753-5766, 2007.
- Robert, Y., Simulation numérique du soudage du TA6V par laser YAG impulsif : caractérisation expérimentale et modélisation des aspects thermomécanique associées à ce procédé. PhD thesis, École des Mines de Paris, 2007.
- Zhang, W., Roy, G.G., Elmer, J.W., and DebRoy, T., Modeling of heat transfer and fluid flow during gas tungsten arc spot welding of low carbon steel. *J. Appl. Phys.*, 93(5):3022-3033, 2003.
- Zhuk, H.V., Kobryn, P.A., and Semiatin, S.L., Influence of heating and solidification conditions on the structure and surface quality of electron-beam melted Ti-6Al-4V ingots. *Journal of Materials Processing Technology*, 190:387-392, 2007.